International Journal of Greenhouse Gas Control 136 (2024) 104189

Contents lists available at ScienceDirect

International Journal of Greenhouse Gas Control

journal homepage: www.elsevier.com/locate/ijggc

Evaluation of safe operating envelope for CO_2 injection under uncertain rock mechanical parameters and earth stresses

Anders Nermoen [a,*], Anton Shchipanov [a], Michal Matloch Porzer [b], Jindřich Šancer [c], Roman Berenblyum [a]

[a] Norwegian Research Center NORCE AS, Nygårdsgaten 112, 5008 Bergen, Norway
[b] Department of Geological Engineering under the Faculty of Mining and Geology at VSB Technical University of Ostrava, Ostrava, Czech Republic
[c] Department of Mining Engineering and Safety under the Faculty of Mining and Geology at VSB Technical University of Ostrava, Ostrava, Czech Republic

ARTICLE INFO

Keywords:
Mechanical stability
CO_2 storage
Safe operating envelope
Strength
Stress
Monte Carlo simulation
Probability of failure
Method development

ABSTRACT

Carbon Capture and Storage (CCS) is a pre-requisite to decarbonize CO_2 emissions from industrial sectors and as an industry capable of compensating for hard-to-abate emissions in a net zero scenario. A method was developed to evaluate the geomechanical constraints and safe operating envelope as function of pore pressure and temperature. The probability of failure was estimated from uncertain input stiffness and strength data, and as cooling and re-pressurization shifts the in-situ effective stresses, the safe operating envelope was determined, here given by pressure and temperature.

Onshore storages nearby industrial clusters enable energy and cost-effective handling of CO_2. In the South-Eastern European region, onshore depleted oil and gas fields located nearby high-emitting industries may developed into CO_2 storages. This paper describes a method for determining maximum fluid pressure as function of temperature from geomechanical restrictions. The method was employed on a practical example used to evaluate the safe operation envelope for a pilot CO_2 injection site into a depleted onshore naturally fractured carbonate oil and gas field. The tool uses Monte Carlo simulations to perform geomechanical stability analyses by sampling from the inherent uncertainty of the input parameters to probability of failure as function of pressure and temperature. The risk of re-opening natural fractures, induced fracturing and fault reactivation are evaluated so the safe operating envelope can be obtained. The uncertainty of the input parameters is thus directly reflected in the safe operating envelope – thus providing an effective communication of value information to external stake holders when maturing a CO_2 storage pilot.

1. Introduction

A green shift towards carbon neutrality as early as possible this century is required since the detrimental consequences of a continued pathway with green-house gas emissions as of today outweighs the societal gains by operating business as usual (Newman and Noi, 2023). A net zero society, where the rise in atmospheric CO_2 concentration is halted, is required due to the longevity of the CO_2 molecule in the atmosphere (Archer and Brovkin, 2008, and Archer et al., 2009). The short-term consequences of a changing climate is already upon us and natural tipping in the climate system may both strengthen and increase the frequency of extreme temperatures, droughts and wild-fires, scarcity of fresh water, floods, ecosystem loss and biodiversity collapse, and soil degradation (Dasgupta, 2021).

To reach net zero CO_2 capture and storage (CCS) is a necessity both to reduce CO_2 emissions from high-intensity emission points, and as an enabler for net negative solutions used to compensate for remaining hard-to-abate emissions.

Having access to certified CO_2 storages is fundamental to any CCS value chain. Onshore storage locations such as depleted oil and gas fields in south-East Europe, located nearby high emission industrialized regions, can provide a significant cost reduction mechanism. Using existing fluid handling and reservoir management competence, surface infrastructure and the potential of retrofitting drilled wells with on-site experienced personnel, all together provide significant cost-reductions.

In the Eastern part of Europe (Parsonsova and Machar, 2021), the demand for decarbonization of heavy industry in product generation is huge. If local industries reduce the emission footprint in a cost-effective

* Corresponding author.
E-mail address: aner@norceresearch.no (A. Nermoen).

https://doi.org/10.1016/j.ijggc.2024.104189
Received 11 December 2023; Received in revised form 15 June 2024; Accepted 23 June 2024
Available online 28 June 2024

way they may continue to compete also in a tightening EU-ETS carbon trading system.

The CO2-SPICER project (Hladik, et al., 2021) was established to kick-start CCS in the Czech Republic. The purposes of the project were (1) to evaluate a depleted oil and gas field, located in the South Moravia region and operated by MND, for a pilot CO_2 injection, (2) to develop competence and gain experience (being a learning platform) for a full-scale injection project, and (3) to identify additional studies required for the pilot and later full-scale injection. The naturally fractured carbonate reservoir in this project is, to the best of our knowledge, the first example of a CO_2 pilot for a depleted carbonate field onshore Europe. This mature field was operated mainly by pressure depletion with limited water injection and is approaching its final production phase. The field may find a secondary use as a CO_2 storage project. Geomechanical stability evaluations, that include the effective stress development during the injection phase, is key to certify the field and to ensure technological safety for local stake holders. Therefore, a method was developed to use the uncertain measurements of stiffness, strengths and Earth stresses to estimate the likelihood of failure as function of pressure and temperature.

Overall, mechanical stability of reservoir rocks is determined by a) evaluating the normal and shear forces projected onto weak planes crosscutting the storage complex (see e.g., Bohloli et al., 2014), and b) evaluating the mechanical strength of the rock material and rock mass in the storage complex to the effective field stresses (see e.g., Park et al. (2022) and Olden et al. (2014)).

MND performed a series of seismic interpretation and geological modelling studies using acoustic and dynamic field data concluding that no major weak fault planes were identified crosscutting the storage location (MND, 2023). Thus, the basic premise of geomechanical evaluation was to evaluate mechanical stability of (1) the matrix rock material itself with results applied to (2) assessment of fractured rock masses.

1.1. *On the geomechanical implication of cooling and pressure increase*

The geomechanical assessment of the change in stress geometry in consequence of temperature was described by Voake et al. (2019) and references there-in. Here, the in-situ stress changes were related to thermal-elastic contraction at uniaxial strain conditions and effective stress changes during the injection of cold CO_2. As detailed in the method section, we assume a uniaxial strain condition (constant reservoir width) and constant overburden stress. Under these assumptions, cooling-induced thermal-elastic contraction reduces the horizontal stresses calculated by Hooke's law for linear thermal-elastic materials in cylindrical coordinates. By employing the Biot's effective stress principle,

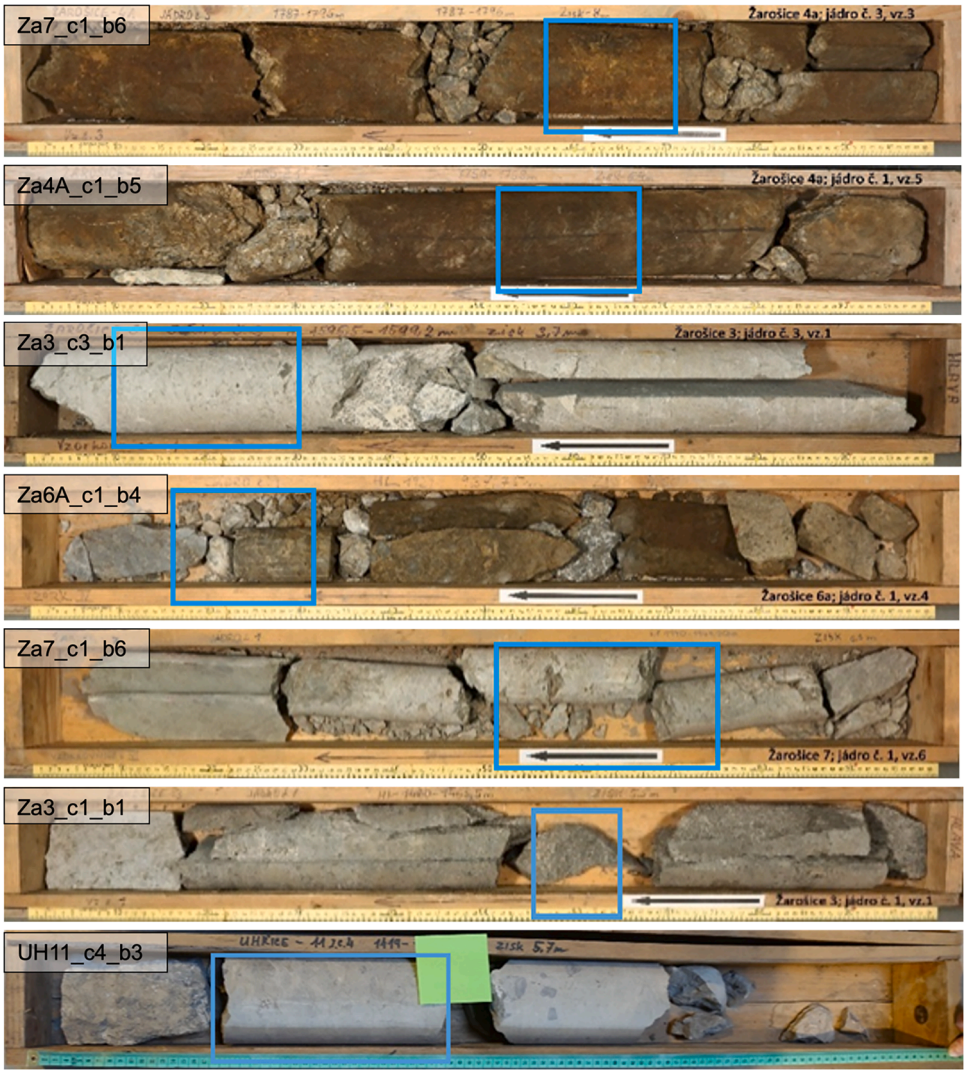

Fig. 1. Picture of the samples acquired from the storage repository. The box number is termed with the field, the well number, core number (jadro) and box number (vz). The blue rectangles depict the samples used in the geomechanical analysis.

the pressure build-up reduces the effective stress. At invariant coordinates, with shear stress along *y*-axis and effective stress along the *x*-axis, a pressure increase shifts the Mohr circle towards failure. Moreover, temperature reduction reduce the least horizontal stress thereby increaseing the radius of the Mohr circle. These effects were included when assessing how temperature and pressure led to stress changes as cold CO_2 is injected.

1.2. Core samples and the origin of uncertainty

Core samples from the different formations represented in the storage complex were acquired by MND and made available to the project in the core repository. Fig. 1 display the significant variation in rock morphology. Only intact core pieces of sufficient size (i.e., that withstood coring, handling, and storage) could be used for geomechanical tests. Thus, a survival bias in the available samples might be expected. However, mechanical weakening could also occur due to the generation of micro cracks in the samples due to e.g. vibrations induced during coring, exhumation, transportation and storage. There is always a lack of sufficient, representative rock samples when performing geomechanical tests, and the value these tests rely on how the rock sample results are applied in the geological context.

Geomechanical stiffnesses parameters of the rock samples (Youngs modulus, Poisson ratio and thermal expansion coefficient), as well as plastic parameters (tensile strength, compaction strength, shear failure strength), and stress data were reported in Nermoen et al. (2024). The observed differences in stiffness and strength of the rock samples, stems from geological variability and experimental uncertainty. Since measurements of Earth stresses were not obtained, but had to be estimated, this adds to the inherent uncertainty of the geomechanical stability analysis.

Previously, similar geomechanical stability evaluations were developed (Berenblyum et al., 2017) was focused on the stability of faults, while thermal effects on horizontal stress were not included. Moreover, the geomechanical parameters were fixed and mainly obtained from the literature. In a recent paper by Voake et al. (2024), the impact of temperature variation on chalk rocks and corresponding stress configuration were studied. In these experiments, the axial load of cylindrical chalk cores was constant, and the minimal horizontal stress was reduced due to cooling at uniaxial strain conditions.

The basic premise of this study is to develop a method that utilize the variability in the uncertain input parameters, including Youngs modulus, Poisson ratio, thermal expansion, mechanical strength, and stress (documented in Nermoen et al. (2024)), to develop a probabilistic geomechanical stability assessment. This is done by Monte Carlo simulations, were the likelihood of failure was estimated for each combination of pressure and temperature. The input data was obtained from random sampling of input data expressed via probability density functions (PDFs). The shape of PDF for each input parameter should ideally arise from the results of a large number of samples. The lack of core material and limitations of laboratory capacity in determining each parameter, the number of data points for each PDF will be limited. This forced pragmatic decisions to be made. When deciding the mathematical nature of the PDF it was decided to a) exclude outliers, b) determine likely minimum and maximum values that define the limits to, c) use uniform PDFs. The subjective choice of PDF for each parameter will impact the results. However, in this evaluation the focus has been to determine the unlikely combinations of drawn parameters that defines the 0.1% and 10% probability failure limit for each pressure and temperature combination.

For each pressure and temperature, the probability of failure was determined by counting the number of unstable realizations, i.e., when the estimated stress level exceeds the failure line at invariant stresses.

Thus, by accounting for thermal effects and re-pressurization the safe operating envelope was determined as reservoir *fluid pressure*, and *temperature* can be controlled by the operator.

When assessing geomechanical stability in Earth systems, the rock mechanical strength of the intact rock samples is applied to fractured rock masses at depth. Fig. 1 display photographs the partly disintegrated core material studied in (Nermoen et al., 2024). It is not known whether the breakage originated from the coring process, exhumation, transport, or storage processes, or was caused by the inherent natural geological variation. By matching core observations with varying logging types of lineation, foliation, fracture density, geologic mineralogical variation of the rock masses can be identified (Hoek and Brown, 1997). Such observations enable a qualitatively, and potentially quantitatively, determination of the apparent strength of the fractured rock masses after which a correction is required to better constrain the stress window of rock-mass stability.

The measured rock-mechanical strengths were compared to conservative choices tectonic stresses (i.e., higher value of vertical stress and lower value of least horizontal stress), and how in-situ stresses change with temperature and pressure to possibly compensate for potential survival bias in the sampling. The probability of failure was determined 4000 times for each temperature and pressure where parameters were drawn from probability density functions for each instance. The safe operation envelope was obtained by choosing a certain probability of failure that may originate from the risk appetite of the operator. The method developed in this paper, has implications to the total storage volume, the rate of CO_2 injection that may be used to calculate e.g. cost-benefit of pre-warming of the injected CO_2 as this would increase the limits of the pore pressure – thus potentially increasing the storage capacity of the field.

2. Material and methods

This section describe the origin of the rock mechanical data and how this data was used to determine the safe operating envelope, i.e., to constrain pore pressure (P_f) and temperature (T) during CO_2 injection.

2.1. Data base of rock mechanical strength

The input data for this study was extracted from the database documented in (Nermoen et al., 2024) where results from the geomechanical test program of stiffness, thermal expansion coefficient and strength parameters from the storage complex were reported. Here, results of 6 reservoir samples and 4 sealing rock samples were used to determine the shear failure envelope. In Table 1, the sample ID, lithology, and true vertical depth from the surface (TVDS) are reported together with the axial (s_1) and radial (s_3) stresses at failure. Here, the samples were loaded axially until failure, while keeping constant $s_3 > 0$ in triaxial tests, and $s_3 = 0$ in unconfined compressive strength (UCS) tests.

2.2. Determining the shear and compaction failure envelope

The failure envelope encapsulates the stresses where irreversible failure of the rock samples occur. This data may be reported in different invariant ways, either as $s_1 s_3$-plots, in shear and normal stress $\tau\sigma$-plots, or in deviatoric and mean effective stress qp'-plots. As described in pp. 79–80 in Fjær et al. (2008) the latter is chosen here, because the Earth stress is expressed as a point instead of a circle in $\tau\sigma'$ space. This eases the computations needed to perform the Monte Carlo probabilistic analysis. In principle, within the elastic domain encapsulated by the failure envelope, the observed deformation is reversible implying that no permanent damage occur during loading and un-loading (Fjær et al., 2008). This does not necessary imply that stress-strain curves during aloading cycle within the elastic domain will always overlap, because of e.g. closure of micro-cracks developed due to exhumation. The deviatoric and mean effective stresses are defined via:

$$q = s_1 - s_3 \tag{1}$$

Table 1
Rock mechanical strength tests using unconfined compressive strength (i.e., when $S_3 = 0$) and triaxial tests ($S_3 > 0$) were performed on reservoir and sealing rocks (from Nermoen, et al., 2024). For each sample the lithology, type, true vertical depth, porosity and dynamic Youngs modulus from sound velocity measurements and permeability is provided. [+]The ZA4A_c3_b3 sample disintegrated and fractured during handling – thus a very low UCS strength is seen. This data point is excluded from the analysis.

Sample ID	Lithology	Type	Depth, TVD (m)	Porosity (%)	Dyn. Youngs mod (MPa)	Permeability (mD)	S_3'(MPa)	S_1'(MPa)
ZA4A_c3_b3_a	Vranovice Fm.	Reservoir	1750.4	3.5	9.8	6.6E+00	0.0	3.1
ZA4A_c3_b3_b				3.8	10.5	1.3E+01	7.0	51.0
ZA4A_c1_b5_a			1724.5	1.3	22.6	9.3E-01	0.0	35.8
ZA3_c3_b1_a			1593.4	1.4	46.9	1.7E-01	0.0	55.2
ZA6A_c1_b4_a			1813.9	1.6	20.7	1.5E+00	0.0	62.0
ZA7_c1_b6_b			1860.5	3.6	34.0	5.8E-01	15.0	165.9
UH11_c4_b3_b	Vranovice Fm.	Reservoir - possible	1394.1	0.6	68.2	1.4E-02	7.0	202.0
UH11_c4_b3_a	Kurd.	analogue		0.3	49.4	3.6E-04	0.0	152.0
ZA3_c1_b1_c	Žarošice Mb.	Seal	1456.68	5.1	61.6	1.4E-02	7.0	145.98
ZA3_c1_b1_b				1.6	48.2	6.4E-02	0.0	43.7
KOE6_c10_b2_a	Myslejovice Fm.		1857.67	3.6	27.1	1.1E-02	0.0	76.9
MIL1_c1_b1_a	Mikulov Fm.		233.78	3.5	40.3	1.4E-01	0.0	49.8

$$p' = \frac{s_1 + s_3}{2} - \alpha_B P_f \quad (2)$$

Here, P_f represents the pore pressure in the reservoir, and $\alpha_B \leq 1$ represent the Biot coefficient (Alam et al., 2012; Nermoen et al., 2013) that suppress how pore pressure changes affect the mean effective stress p'.

The deviatoric (q) and mean effective stresses (p') at failure, from both UCS tests and triaxial tests on reservoir and sealing rock samples are, respectively, shown as circles and squares in Fig. 2. The true vertical depth from surface were used as data labels to identify each sample.

As may be seen in Fig. 2, there is sample variability, and thus implicit flexibility which shear failure curve to use when evaluating mechanical stability. Stability analysis was performed on two cases, namely the strength envelope from all samples (solid line) and from samples acquired from 1724 to 1740 m depth (long dashed). In all, the shear strengths of the sealing were higher than the reservoir samples.

Fig. 3 display the strength data in Table 1 as Mohr-circle plots. The Mohr Coulomb shear failure line was derived to best tangential fit the

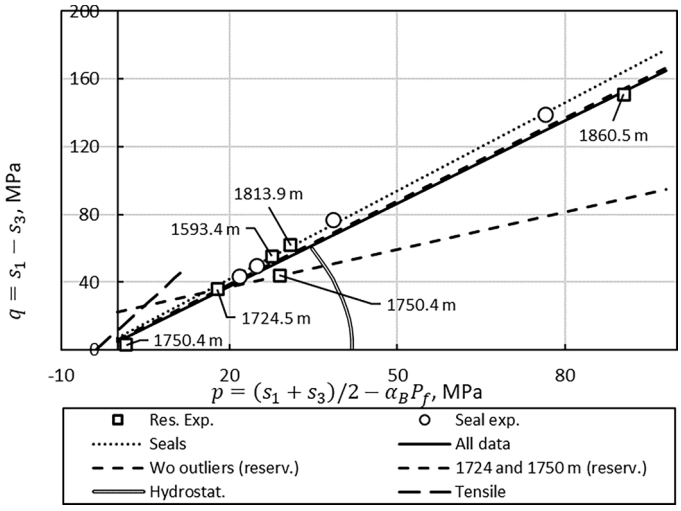

Fig. 2. Failure envelope in qp-plots from rock-mechanical tests. Tensile strength from Brazilian tests to the left (long dashed), compaction failure for hydrostatic stress tests on the right (double line) and shear failure for sealing (circles) and reservoir rocks (squares) from UCS and triaxial tests. The depth from surface for each sample for UCS and 3ax displayed as data labels (for reservoirs). Three lines were drawn where solid line entails all reservoir tests, the dashed line for seals, and the long-dashed line for samples from 1750 to 1724 m depths. Slope and intercepts are 1.63&4.7, 1.64&6.0, 0.73&22.5 MPa for the reservoirs, and 1.73&7.3 MPa for seals – being systematically stronger.

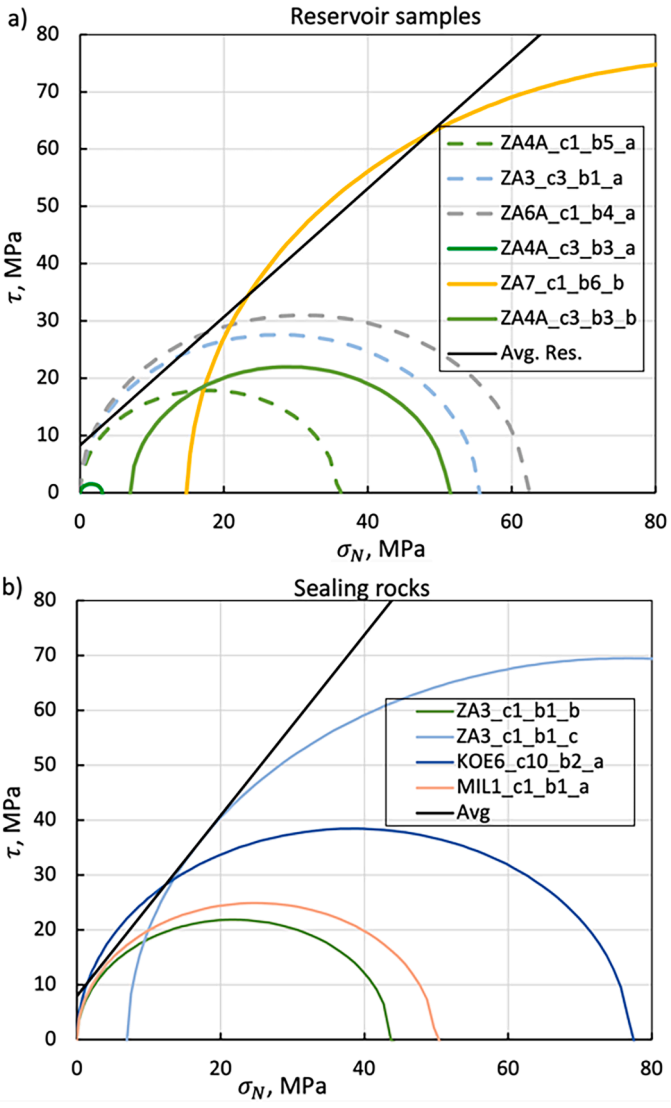

Fig. 3. Mohr Coulomb failure envelope of reservoir and sealing rock samples. Average intercept of the Mohr circles is displayed so that assessment of Cohesion and slope can be obtained. These data are equivalent to the strengths displayed in Fig. 2.

different Mohr-circles for reservoir and sealing rocks, in a) and b), respectively. As can be seen, the variation in strength between samples was significant. Cohesion of 8.3 and 8.0 MPa, and slope of 1.6 and 1.1 were obtained for sealing and reservoir rock types, respectively, displaying how sealing rocks were stronger than the reservoir rocks samples.

2.3. Hydrostatic loading experiments

22 samples, from the main lithologies represented in the reservoir complex, were exposed to hydrostatic confining pressure tests with peak stresses up to 43 MPa. The Coreval 700 tool as reported in (Nermoen et al., 2024), were used to measure how pore volume and permeability varied with confining stress enabling a comparison of loading and un-loading paths in stress-strain plots. Typically, if un-loading path differs significantly from the loading, this was attributed to irreversible damage. Significant variation was seen for one sample, while for the remaining 21 samples, the unloading path followed the loading path indicating a compressive strength exceeding 42 MPa (indicated by the double line in Fig. 2).

2.4. Determining tensile strength envelope in qp-space

Tensile strengths were determined with Brazilian tests on 23 rock samples from different parts of the storage complex (Nermoen, et al., 2024). An average tensile strength (T_0) of 3.9±1.8 MPa and 6.0 ± 2.2 MPa was provided for the reservoir rocks and sealing rocks, respectively.

In *qp*-plots the tensile stress is drawn as a slanted line (Fig. 2). In reservoir settings, pre-existing tensile fractures with their surface normal parallel to the minimum horizontal effective stress will re-open when the total effective stress becomes negative. Moreover, new fractures will develop when the effective stress is less than minus T_0 (tensile strength). In a reservoir setting, this occurs typically by pore pressure buildup or due to tectonic rifts. By using the effective stress relation (Eqn. (2)), tensile fractures form when the following stress condition is met:

$$T_0 \geq s_3 - \alpha_B P_f \Rightarrow P_f \geq \frac{s_3 + T_0}{\alpha_B} \tag{3}$$

As such, pore pressure must exceed the least in-situ stress plus the tensile strength divided by the Biot coefficient to initiate failure. If, pre-existing fractures exist in the reservoir, they will re-open when,

$$P_f \geq \frac{s_3}{\alpha_B} \tag{4}$$

One may calculate this requirement in qp'''-space by re-shuffling the tensile crack criterion to $s_3 = -T_0 + \alpha_B P_f$, and use this in the qp' definitions in Eqn (1) and 2,

$$q = s_1 + T_0 - \alpha_B P_f \qquad p' = \frac{1}{2}\left(s_1 - T_0 - \alpha_B P_f\right) \tag{5}$$

This criterion enables the tensile strength envelope to be drawn in qp'-plots from T_0 measurements.

2.5. Thermal-elastic stiffness constants

Elastic constants were derived from 72 ultrasonic velocity tests, hydrostatic cycling tests, and thermal expansion determination (Nermoen et al., 2024). The results vary, and for the analysis presented here, the results were intended to apply to the overall reservoir. Some of the observed variation was dictated by petrophysical characteristics enabling adjustments to be done to what is more likely to be relevant for the reservoir overall. This adjustment was performed to improve the credibility of the estimates. The stiffness and strengths correlated with porosity, exemplified in Fig. 10A in (Nermoen et al., 2024), where the bulk modulus (K) correlated with porosity. Given that the reservoir has a porosity in the range of 8–10% (MND, 2023), adjustments had to be done, so a bulk modulus in the range 4–6 GPa was therefore used on the reservoir scale. Further, the data displayed no correlation with porosity for neither Poisson's ratio nor Biot coefficient, as such the average and standard deviation were used directly, i.e., $\nu = 0.35 \pm 0.04$ and $\alpha_B = 0.85 \pm 0.07$. Further, the thermal expansion coefficient and Biot coefficient was measured. Table 2 provides an oversight of the input parameters that was used determine the relation between temperature, pore pressure and the shifts the in-situ stresses in the tool.

2.6. Determining earth stresses at depth

Mechanical stability at a given depth rely on the mechanical strengths and the invariant combination of the largest and smallest principal stresses, s_1 and s_3, respectively. The principal stresses were not measured in the reservoir complex in focus. Estimates were obtained in three ways:

1. The vertical weight of the overburden can be assumed from average density via $s_1 = \rho_{avg} g h$. If the reservoir body is held on its lateral sides, and the top surface is free we may use the uniaxial strain assumption (i.e., its lateral length is constant), in Hooke's law to determine the minimal horizontal stress via $s_3 = s_1 \nu/(1-\nu)$.
2. By assuming that the stresses measured in three coal mines located 140 km away from the storage complex are the same (Staš et al., 2003) one may linearly extrapolate the stresses to the desired depth. The validity relies on assuming comparable lithology and similar tectonic setting. This may be debatable, however, by using the measurements from ca. 750 to 950 m depths (see Fig. 14 in (Nermoen et al. 2024) and extrapolate to 1750 m depths, the largest and smallest principal stress can be determined with uncertainty.
3. By analysing breakouts in well, one may estimate the range of the two horizontal stresses from using the techniques developed by (Zoback et al., 1986 and Zoback et al., 2003).

There is significant inherent uncertainty in this method so that the value of s_1 and s_3 used in the analysis was 41.7±1.0 and 23.0±1.5 MPa with a flat probability distribution function (Table 2). These estimates are also displayed in Fig. 4.

2.7. Estimating earth stress changes during injection of cold CO_2

The equations used to estimate how Biot effective stress and thermal-elastic processes modify the Earth stress due to pressure build-up and cooling is shown here. In weight dominated systems the vertical stress (s_1) remains constant. If the reservoir has a constant width (i.e., uniaxial strain assumption) where the tectonic forces balance the reservoir flexure in the horizontal direction, thermal contraction reduces the

Table 2
Upper and lower bound of geomechanical input parameters used in the Monte Carlo simulation. A square distribution is used with equal probability within the limits. The variability is linked to the geomechanical experiments on reservoir samples in Nermoen et al., 2024. A flat probability distribution was used. The upper and lower bound of the thermal-elastic coupling parameter β_T is estimated from 1 000 Monte Carlo runs drawing from the distribution of Poisson's ratio, Youngs modulus and thermal expansion coefficient in Eqn. (6).

Parameter (annotation), unit	Lower	Upper
Thermal expansion coefficient (α_T), K^{-1}	1.30E-05	2.70E-05
Bulk modulus at 8% porosity (K), MPa	4000	6000
Poisson ratio (ν), 1	0.31	0.39
Biot coefficient (α_B), 1	0.78	0.92
Maximum in-situ stress (σ_1), MPa	40.0	42.0
Minimum in-situ stress (σ_3), MPa	20.6	23.6
Initial pore pressure (P_f), MPa	17.0	18.0
Thermoelastic coupling coefficient (β_T), MPa K^{-1}	0.101	0.176

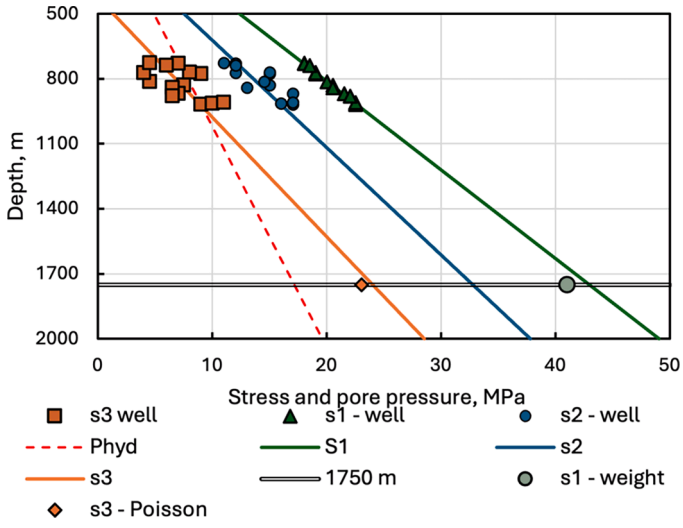

Fig. 4. Principal stresses measured nearby in coal mines, Ostrava (Staš, Kolcun, Simkovicova, and Soucek, 2003) at depths of 700–1000 m, extrapolated to 1750 TVDS. The slopes in stresses were 18.1, 20.2 and 24.4 kPa/m for s_3, s_2 and s_1, respectively. The estimated weight of the overburden and minimum and maximum horizontal stress (from Poisson coefficient of 0.35) shown as diamonds and circle. Figure acquired from (Nermoen et al., 2024) (break out analyses omitted here).

minimal horizontal stress (s_3). By employing fixed vertical principal stress, uniaxial strain in the horizontal direction, and linear thermal-elastic Hooke's law, the change in the minimum horizontal stress (Δs_3) can be linked to temperature changes (ΔT) via (e.g. (Voake, et al., 2019, and Voake, 2020):

$$\Delta s_3 = \frac{E\alpha_T}{1-\nu}\Delta T \tag{6}$$

Since Youngs modulus is related to bulk modulus and Poisson ratio,

$$E = 3K(1-2\nu), \tag{7}$$

one may estimate the minimum horizontal stress reduction from measurements in bulk modulus, Poisson ratio, thermal expansion coefficient and the amount of cooling, via:

$$\Delta s_3 = 3K\alpha_T\frac{1-2\nu}{1-\nu}\Delta T = \beta_T\Delta T \tag{8}$$

An average value of the coupling coefficient $\beta_T = 0.14$ MPa·K-1 is obtained from $K = 5000$ MPa, $\alpha_T = 2{\cdot}10^{-5}$ K-1 and $\nu = 0.35$. By sampling from experimental variability in the thermal-elastic parameters, the coupling coefficient between temperature and minimum horizontal stress range between 0.10 and 0.17 MPa·K-1 (Table 2). This implies that by reducing temperature by 1 °C the total minimal horizontal stress is reduced by 0.14 MPa.

This shift in stress is displayed in *qp*-space in Fig. 5 where the value of p' reduced and q increase, thus shifting the estimated stress-could in the north-west direction. This is mathematically equivalent to analyzing Mohr circles in $\tau\sigma$-space, when by keeping vertical stress constant and reducing the minimum horizontal stress increase the radius (Fig. 6).

A flat probability density function (PDF) was employed for all input parameters in the simulation. Each PDF was constrained by an upper and lower limit for each parameter obtained by the experiments and estimates. The flat distribution was used since the necessary number of high-quality data points needed to establish a well-defined average and standard deviation was insufficient. In principle any probability density function can be applied in the technique developed for Excel.

Increasing pore pressure reduces the value of p' (Eqn. (2)) by a factor proportional to the Biot coefficient; thus, shifting the stress state west. Thermal contraction reduce of s_3 thereby reducing p and increasing q

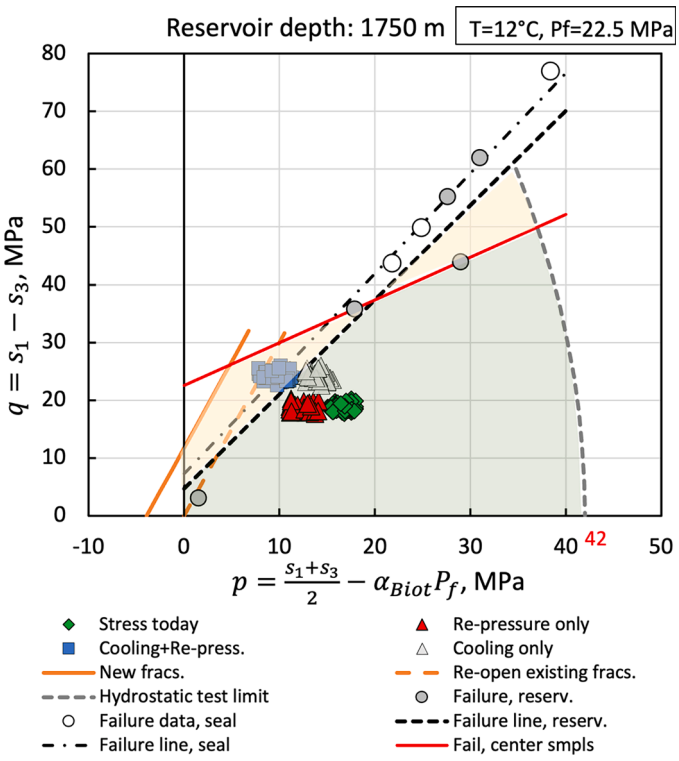

Fig. 5. Plot of rock strength data in Table 1 with Earth stresses. UCS and triaxial strengths from seal (open) and reservoir (grey circles) in *qp*-space with best fit as long dash and dash-dot for seals. Two samples in the centre of the reservoir at 1724 and 1750 m TVDS are shown with short dashed line. Brazilian tensile strengths for reservoir rocks in orange solid line, and the stress state with zero tensile strength, i.e. re-open existing fractures is shown as dashed line using Eqn. (3)-(5). Hydrostatic test limit with confining pressure up to 42 MPa to the right (grey dashed line). The green shaded areas display the safe operating envelope, while the yellow shaded area is subject to choose relevant strength envelope. Green diamonds display the initial stresses (in Table 2), at 52 °C and 17.5 MPa, red triangle the effect of re-pressurization, diamonds the effect of cooling, and blue squares the combined effect.

(Eqn. (1) and Eqn. (2)). In *qp*-space, cooling shifts the stress state in the north-west direction. In $\tau\sigma$-space, a pressure increase does not change the radius of the Mohr circle, but rather shifts it towards the failure line.

In essence, both re-pressurization and cooling bring the stress towards the failure line.

2.8. *Representing the earth stress and failure envelope in qp-space and τσ-space*

The advantage of using *qp*-space when evaluating geomechanical stability is that the estimated Earth stresses is displayed as points instead of circles. If these points exceed the failure envelope, the reservoir was deemed geomechanically unstable. The different failure envelopes obtained from rock-mechanical tests are shown in Fig. 5, including tensile strength of reservoir samples, and the shear failure of reservoir and sealing samples. Depending upon where in the reservoir stability is evaluated, different failure lines and stresses should be used. In Fig. 5, the green shaded area represents the safe envelope, while the yellow zone is subject to choice.

When evaluating geomechanical stability of the storage complex it was decided to limit the analysis by considering the reservoir rocks – being the weakest formation. Moreover, this is where cooling and re-pressurization, and thus the shifts in stress level, will occur.

Given the variability in initial stress and pressure ranges, we sampled from the distributions of stresses, pore pressures, Biot coefficient, and thermal-elastic coupling coefficient to evaluate how stress changed as

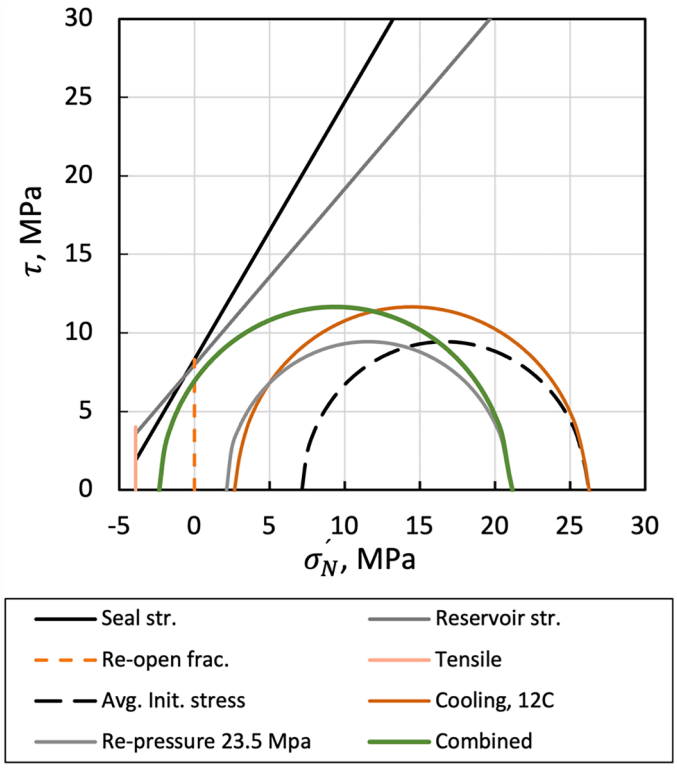

Fig. 6. Same strength data as used in Fig. 5 has been plotted here with tensile strength of reservoirs, re-open pre-existing fractures with zero tensile strength (dashed line), shear strength of seals and reservoir. The Mohr circles display the average reservoir stress and pressure (black dashed), re-pressure in grey, cooling in orange, and the combined effect in green.

function of changes in temperature and pressure. Fig. 5 display these effects, and depending upon the relevant failure line, the likelihood of failure was evaluated.

Significant variability in the representative rock strengths and Earth stresses can thus be analysed depending upon subjective choices.

The exact same failure data, and stress and pressure level as shown in Fig. 5, is visualized in Mohr Coulomb plot in Fig. 6. The combined effect of cooling and re-pressurization is expected to re-open tensile failure, but the shear failure line seems un-touched by the Mohr circle. In Fig. 5, however, the Monte Carlo simulation sampling from the inherent experimental and geological variability in the input parameters allow for automatic counting of unstable instances so a quantitative estimate of risk, given pressure and temperature condition, can be obtained.

3. Monte Carlo simulation procedure

Monte Carlo simulations were developed to use the experimental and geological uncertainty to determine the probability of geomechanical failure as function of how Earth stresses change with pressure and temperature. The simulations were developed in Excel using data tables to analyse mechanical stability combinations of 20 pressure instances and 12 temperature instances. For each combination, geomechanical stability was evaluated 4 000 times. For each evaluation a unique set of parameters were drawn from probability density functions (PDFs) of: stresses (s_1 and s_3), initial pressure, Biot coefficient (α_B), and thermal-elastic coupling coefficient (with upper and lower values of the flat PDFs shown in Table 2. For each of the evaluations in each pair of pressure and temperature, the shifts in effective stresses were calculated using Eqn. (1) and Eqn. (2) in combination with Eqn. (8) and compared to the failure envelope for stability evaluation. Since the evaluation was performed in *qp*-space, the number of stress configurations that exceeded the strength envelope define the probability of failure.

The input parameters, i.e., Biot coefficient, maximal vertical and minimal horizontal stress, and pore pressure, were uncertain (Table 2), this leads to a "cloud of stresses" in *qp*-space before at in-situ conditions. When cooling and pressurization is included, the additional variability in thermal-elastic coupling coefficient leads to a larger span of the cloud in stresses (Fig. 7a).

Since the input parameters were drawn from PDFs, the same pressure and temperature could have points that would exist both above and below the failure line. As temperature reduced and pressure increased, a gradual increase in probability of failure from safe till unsafe was calculated. If all parameters were fixed, the shift from safe till unsafe would be a 2D step-function.

Pressure and temperature were then systematically varied and based on the shifts in stresses, mechanical stability was evaluated, and probability of failure was determined. Fig. 7a displays individual impact of cooling and re-pressure on the stresses when compared to the initial stresses in green, and the combined effect in grey. In the concrete example, a failure probability of 99.6% is estimated if the pore pressure is increased to 25.5 MPa and temperature is reduced from current 52 °C to 27 °C. Here, the dashed shear failure line is the average of all reservoir shear strength failure tests.

The Monte Carlo simulation used in this study was performed with four different failure lines as shown in Fig. 5: a) Tensile strength, b) re-open pre-existing fractures, c) Mohr-Coulomb friction for all reservoir samples and d) the two samples located at 1724 and 1750 m TVDS.

The tool thus allows for assessing geomechanical risks both due to a deliberate choice of failure line, and an integrated use of the natural variation in experimental and geological parameters. The tool allows for including variability in a transparent and statistically realistic way, so the probability of failure can be expressed depending on pressure and temperature (Fig. 7b) depending on natural variation and subjective choice. In this case, if the reservoir is maintained at 52 °C, the maximal pore pressure could increase to 25–26 MPa, while if it is cooled down to 12 °C the critical pressure would be reduced to 19 MPa.

The method developed here is non-dimensional in time and space. In a realistic scenario injection of CO_2 leads to changes in pressure and temperature through time and space. Depending upon e.g., the thermal heat capacities, multiphase flow field, and boundary conditions the pressure and temperature field will change through time and space. In consequence, the evaluation developed here could be calculated at each point in space.

4. Evaluating the safe operating envelope for CO_2 injection

4.1. The safe operating envelope

The likelihood of failure as function of pressure and temperature relies on a range of user-defined parameters that may be considered subjective. By selecting the adequate failure mode and modifying the PDFs of the input parameters as new information is gathered on the field, probability of failure as function of pressure and temperature will change. Moreover, by assessing the risk appetite of the storage operator one may determine the acceptable failure probability (see slated lines in Fig. 7b). This assessment would arise from a balance between the value added by injecting more CO_2 and the costs associated with the risks of failure.

Even when rock mechanical tests and field stresses will be evaluated in the best possible way, there are always deliberate choices to be made on e.g. choosing which data points to include. The tool enables the developer to evaluate the consequences of such choices – which in turn determines the storage capacity of the field.

As an example, in Fig. 7a all the rock mechanical shear failure strength tests were used. If only we were considering the strengths tests from 1724 to 1750 m TVDS (long-dashed line in Fig. 2), the output of the stability analysis would be quite different (Fig. 8a). Here, cooling and re-pressurization lead to both shear failure, re-open pre-existing fractures,

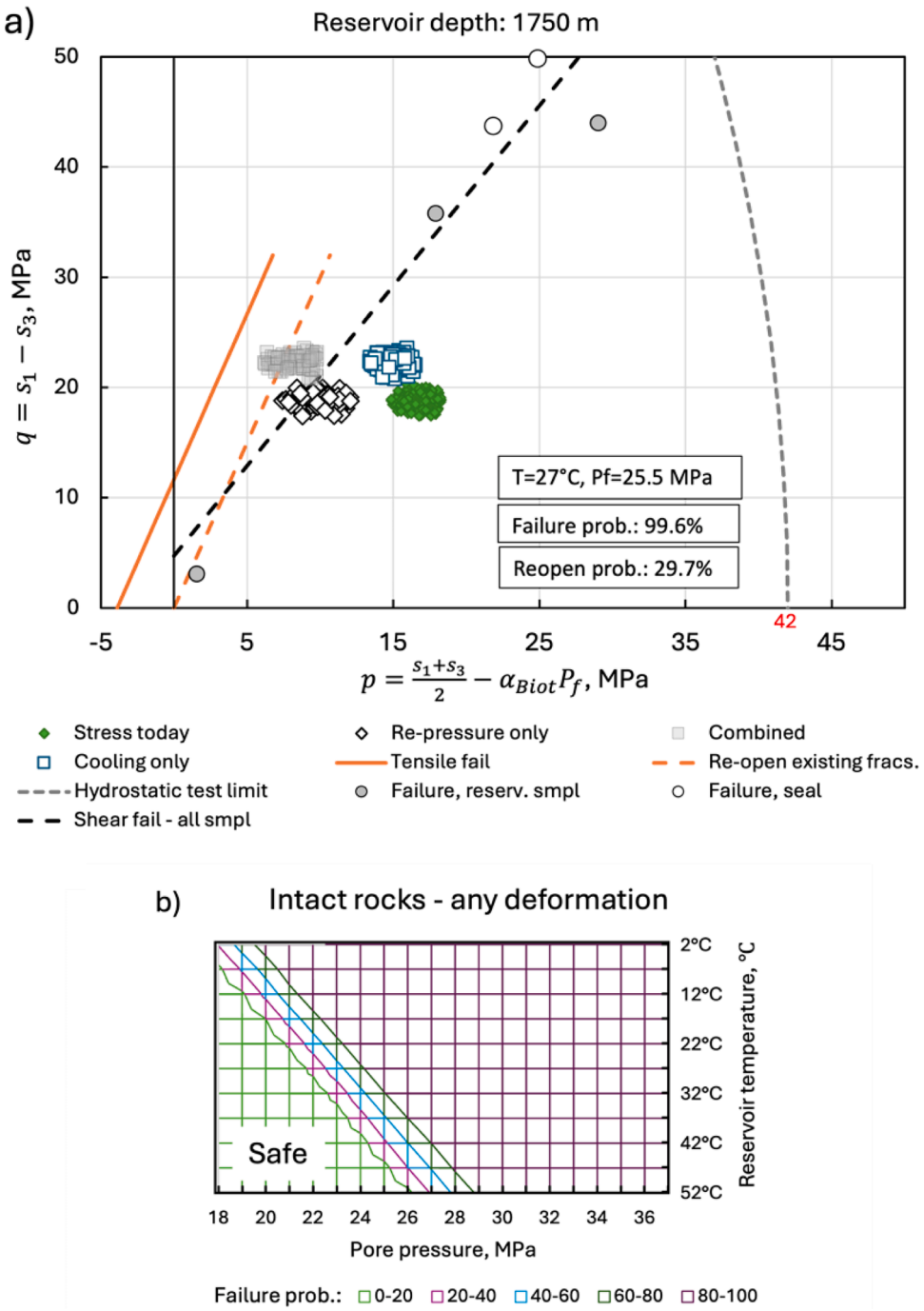

Fig. 7. a) Plot of failure envelope (tensile strength) and shear failure based on all reservoir samples and tectonic stresses in *qp*-space. Green 'cloud' display the initial stresses at 52 °C and 17.2 MPa. The impact of re-pressurization to 25.5 MPa (yellow), cooling to 27 °C (orange), and combined (grey) is displayed. The number of realizations above the specific failure line determine the probability of failure. b) By systematic variation in pressure and temperature and the probability of fialure, here based on the failure envelope in a), can be calculated. Safe operation window in green, based on counting the number of instances exceeding the dashed line in a) (all samples).

and, if these pre-existing fractures do not exist near the injector, to initiate new tensile fractures. As the example in Fig. 8a display; at 27 °C and pore pressure of 25.5 MPa, the number of stress instances leading to failure of intact rocks was zero, but the number of instances that would re-open existing fractures was 29.7%.

When running through all pore pressure and temperature cases, sampling from 4 000 instances from each combination of P and T, the probability of failure of intact rock can be obtained (Fig. 8b). Here, the safe operating envelope, with a low probability of failure is larger than in Fig. 7b.

When compared to the likelihood of re-opening pre-existing fractures (zero tensile strength T_0) in Fig. 8c, the probability as function of P_f and T is shifted to the left. The difference between Fig. 8b and c may be used to investigate at which pressure pre-existing fractures may be opened. This is relevant in the field in focus that is already fractured.

The fracture opening pressure (for a given temperature) may be used as the maximum injection pressure in planning CO_2 injection operations. In some cases, such fracture reopening may be allowed providing better flow capacity of the reservoir. In dynamic reservoir simulations (e.g. (Shchipanov, Kollbotn, Surguchev, and Thomas, 2010)), one may use

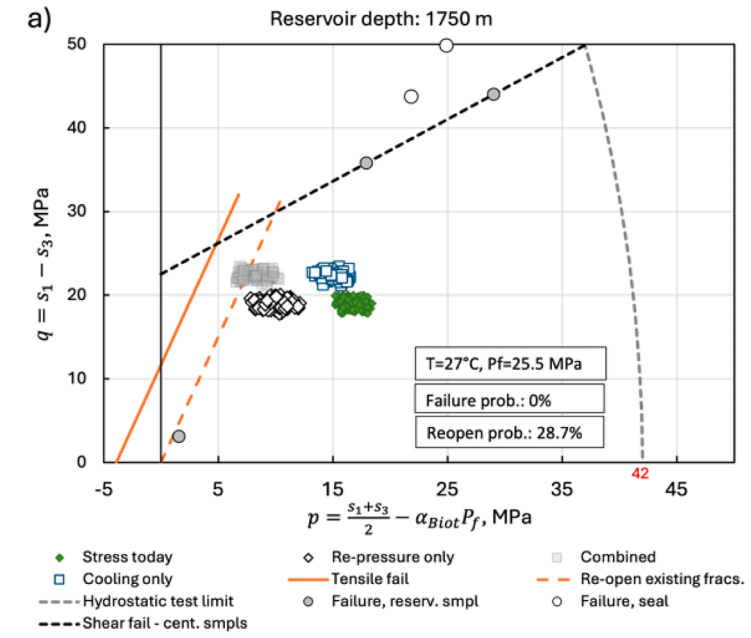

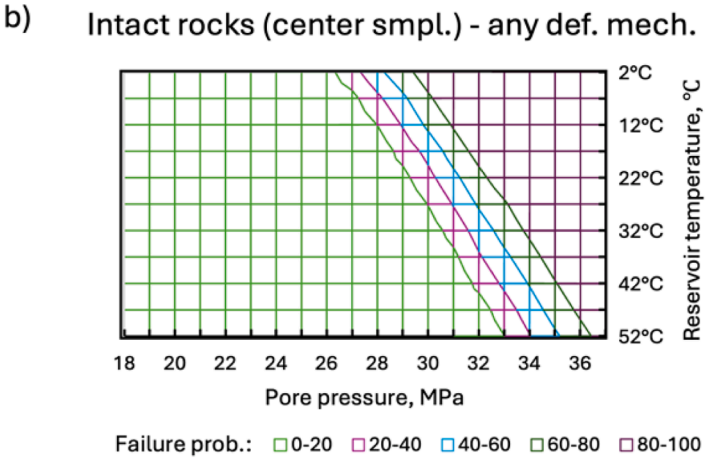

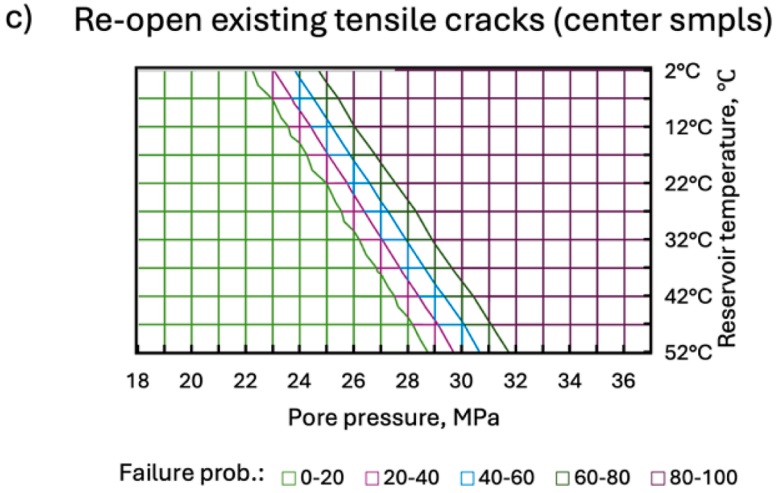

Fig. 8. Shear failure analysis based on experiments on rock samples placed in 1724 and 1750 TVDS. a) An example of cooling and re-pressurization to 27 °C and 25.5 MPa (same as Fig. 7) display that the probability of failure is zero, although the likelihood of re-opening pre-existing fractures with their surface normal parallel to s_3 is determined to be 7.1%. In b) the probability of inducing failure to intact rock samples are calculated for all pressure and temperature cases. In c) the probability to re-open existing fractures (is any) is shown. Safe operation window in green.

this fracture opening via introducing pressure-dependant permeability and evaluating related well injectivity variations during injection operation. Improving flow capacity of the reservoir in this case may increase injection rate and capacity attainable with reducing the energy consumption at the same time without doing additional harm to the already fractured carbonate reservoir.

When assessing the difference between the curves in Fig. 8b and c, we may choose isocontours in probability of failure of 0.1% and 10% to obtain the critical pressure as function of temperature. An ideal injection pressure may thus be estimated by including the potential advantages by re-opening existing fractures to boost injectivity, and the risks of generating new fractures that may lead to leakage of CO_2 out of the target formation. This, also depends on the risk appetite of the operator as shown in Fig. 9.

4.2. Relative importance of input parameters to safe operating envelope

We present here the results of a sensitivity analysis that investigate the relative importance of the various input parameters that dictate the size of the operating envelope (Fig. 9). The size of the operation envelope consists of the number of pressure and temperature instances with a failure probability less than 10%. The analysis was performed on the rock strength originating from all reservoir samples in Table 1 (i.e., dashed line in Fig. 7). The purpose was to determine the most sensitive input parameters, that may guide further work.

The size of the safe region in P_fT-space (with pressure ranging from 17.2 to 36.2 MPa in 1 MPa steps and temperature from 55 to 10 °C in 5 °C steps) is measured by assigning low, medium, and high value of each parameter. Each parameter is changed individually, while keeping the other input parameters at the mean value. The size of the safe regions is summarized in Table 3. The safe region when all input parameters are at medium value is 20.8% serving as a comparative basis for the other permutations.

Varying the thermal expansion coefficient from $2{\cdot}10^{-5}$MPa·K^{-1} to 1 and $3{\cdot}10^{-5}$MPa·K^{-1}, changes the safe region to 32.9% and 15.0%, respectively. Increasing thermal expansion coefficient increases the s_3-sensitivity to temperature change, thus a given cooling leads to a larger change to least effective stress. This brings the stress 'cloud' towards the failure envelope, i.e., the radius of the Mohr Circle increase. A similar effect is seen for the bulk modulus. Considering the Poisson ratio, the impact is more complex as it affects several components of the calculation. In this case a reduction from 0.35 to 0.31 reduce the size of the safe region. This is also the case with Biot coefficient, that when being lowered reduces the impact of pore pressure buildup. In Table 3, the thermal expansion coefficient would be the dominant parameter controlling the safe operation window. This may, however, be a function of the assumed PDFs of initial effective reference stress, rock strength etc., thus this conclusion might be different in other settings.

Table 3
Measure the size of the safe operation window compared to the total span in P and T space. The average of all parameters (as shown in Table 2) was giving a score of 20.83%. By varying each parameter up or low, of the safe operation window either increase or decrease. The change in percentage points compared to average are shown. The operation window is defined with a probability less than 10% of failure.

All parameters average	20.83%		Size of safe operation window	Change in percentage points
Thermal expansion coefficient	Low	1.00E-05	32.9%	12.1%
	High	3.00E-05	15.0%	−5.8%
Bulk modulus	Low	5000	23.8%	2.9%
	High	7000	18.8%	−2.1%
Poisson ratio	Low	0.31	18.3%	−2.5%
	High	0.39	25.4%	4.6%
Biot coefficient	Low	0.78	28.8%	7.9%
	High	0.92	17.5%	−3.3%
Largest principal stress, s1	Low	40	21.7%	0.8%
	High	42	20.4%	−0.4%
Least principal stress, s3	Low	21.3	14.2%	−6.7%
	High	24.3	27.5%	6.7%

Equally, if more precise data for principal stresses also changes the size of the safe operation window during injection of CO_2.

Further tailor-made evaluation programs may focus on determining thermal expansion coefficient and minimum horizontal stress as being most influential to determine the safe operation window – that dictate the safe injected volumes. This approach enables the operator to determine the value of new information.

5. Discussion

When using stability analyses, as shown here, it is important to realize that the analysis is only valid up until failure. Post failure mechanisms include both material strength degradation due to

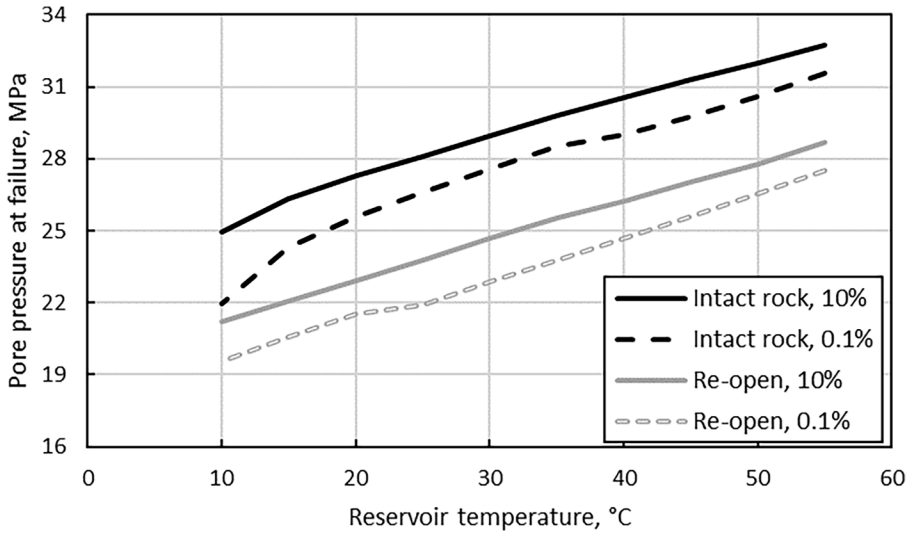

Fig. 9. Pore pressure at which deformation of intact rock, and re-opening of existing fractures as a function of temperature. The critical pore pressure is obtained from 0.1% and 10% probability of failure. The risk appetite of the operator, i.e., if the storage operator accepts higher risks of failure, affects the assessment of maximum pore pressure. The input parameters are shown in Table 1, and with the failure lines in Fig. 8a.

deformation and a re-calculation of stresses and stress directions. Such effects were not studied. The method developed here does not take into consideration the fact that both pressure and temperature will change through time and space. Clearly, the method could be utilized in multiphase flow models modelling the propagation of pressure and temperature fronts to determine when and where within the reservoir the risks of failure may rise. This coupling is outside the scope of this paper.

5.1. Rock sample properties and its relation to rock masses

Evaluating the geomechanical strength of intact rock samples is crucial for understanding rock mass behaviour under in-situ conditions. However, the sampling process may be subject to a survival bias, as fractured or weaker core samples often disintegrate en route, leaving primarily intact samples for geomechanical laboratory study. This poses a challenge, as geological materials display variability at scales from millimeters to meters, even within the same formation. Consequently, there's a valid concern about whether these stronger samples accurately represent the true strength of the rock mass, especially when considering reservoir heterogeneity. Moreover, the influence of fractures and voids on the geomechanical properties of both chemically and mechanically altered rocks warrants further investigation.

Upscaling the geomechanical results of rock samples to fractured rock masses has been a long-standing issue in the application of laboratory rock tests geomechanical tests in reservoir modelling. There are a range of geomechanical classification methods that can be used, such as the GSI Hoek Brown (Eberhardt, 2012; Hoek and Brown, 1997) and the Q Barton system (Barton et al., 1974). These methods quantitatively account for the fracture impact based on scaling coefficients representing fracture properties (intensity / spacing, orientation etc.). These fracture properties may be estimated from interpretations of relevant outcrop data, well logging (like FMS / FMI logs) with further conditioning to dynamic field data (like well tests and well monitoring data) (Bourbiaux et al., 2002; Shchipanov et al., 2006).

As an example, presence of fractures, foliation, etc. leads to a reduced mechanical strength of the rock mass. A detailed study has not been conducted here, however, the impact is illustrated in Fig. 10, where the axial stress at failure, failure strength for each sample in Table 1, is reduced by 40%. This shifts the failure stress in *qp*-space from the black (original) to the blue (adjusted) line. Thus, the position of the failure envelope is shifted (blue curves). The difference is marked by the blue and orange shaded regions consequently reducing the safe operating envelope. Further studies are required to determine the appropriate adjustment from intact rock-samples to overall rock-mass perspective.

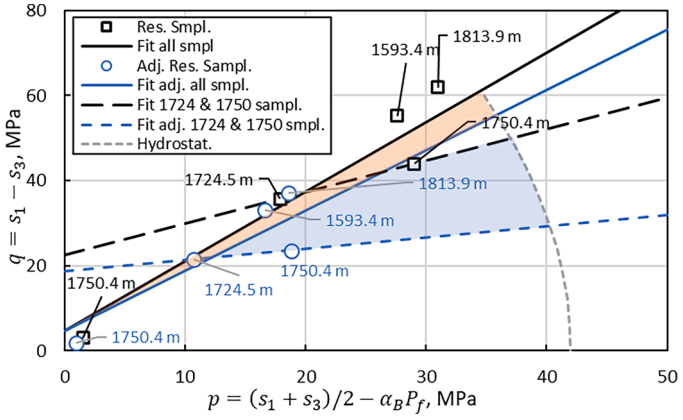

Fig. 10. An illustration of how the failure envelope obtained from the mechanical tests of intact rock samples (black) may change for rock masses (blue), when applied to *qp*′-space. The adjustment is performed by reducing the axial load at failure by 35%.

This effect adds another uncertainty in the analysis of limitations to the injection program for future CO_2 injection operations.

5.2. Risk appetite and geomechanics

The cooling induced thermal contraction and minimal horizontal stress reduction and re-pressurization by CO_2 injection represent the geomechanical constraints to the injection program. Depending upon risk appetite of the injection operator, the analysis above can be used to determine the maximum pressure which in-turn govern the ultimate CO_2 volumes to be safely stored. If cooling shows to be an important limiting factor this may limit injection rate even though e.g., high injection rates are attainable due to high reservoir flow capacity and large volumens needed available for injection. One may need to consider preconditioning (heating-up) of the injected CO_2 or slow the injection rate to eliminate such effects. The reservoir cooling depend on the thermal heat capacities of the rocks and the fluids present before injection starts and the way in which the fluids mobilize or mixes with the injected CO_2 as well as the relative importance of advection and diffusion as dominating mechanisms for cooling through time and space. Warming up the injected fluids increase the safe reservoir pressure.

The operators risk appetite will also depend on estimates of the fate of the injected fluids, if e.g., they migrate out of the target formation, as well as if the site is being monitored and what remedial action plans that can be mobilized if unwanted scenarios are encountered.

As an example of application of the envelope presented above (Fig. 9), assuming the risk appetite of 10% of failure is acceptable, the maximum injection pressure is around 28 MPa, if the injected CO_2 is preheated to 55 °C. If, however, the system is cooled down to e.g., 10 °C the maximum injection pressures were as low as 22 MPa. A balanced analysis must be performed by evaluating the value of increasing the total uptake of CO_2 in the reservoir to the cost of heating. This constrains the whole capture, transport, and storage CCS value-chain.

Reservoir fluid flow simulations may determine the impact of cooling through time and space by using realistic saturation and temperature profiles. The corresponding variations in PVT properties of the relevant formation fluid mixtures, as function of pressure and temperature dictate the overall injection capacity. Moreover, dissolution of CO_2 into the other formation fluids, and fluid migration out of the reservoir body into eventual aquifers play a role.

5.3. Compensation to survival bias

Throughout the geomechanical stability analysis, conservative choices were made to compensate for the possible survival bias in the core sampling. Firstly, the overall variability in the earth stresses is likely to be over-estimated, as both stress-arching and lowered densities in the uppermost sections of the overburden can be expected.

Furthermore, the presence of an intermediate lateral stress (s_2) has been shown to stabilize the mechanical strengths, as truly poly-axial stress experiments revealed that the axial stress at failure is larger when $\sigma_2 > \sigma_3$ than when $\sigma_2 = \sigma_3$. The latter is assumed here so that the likelihood of failure could be over-estimated (Fjær, et al., 2008).

Moreover, the value of the thermo-elastic coupling coefficient seems to be larger than what has been reported by other authors in the scientific literature on carbonates as reviewed by (Voake, 2020). Lowering the thermal elastic coupling coefficient would reduce the sensitivity to cooling.

5.4. Impact of varying uncertainty in the input parameters

The steepness of the curve, from 0 to 100% failure depends solely on the widths of the probability density functions (PDFs) that are fed into the analysis tool. As more data is collected, the uncertainty may either increase or decrease, because of the natural variability of the data itself. More data would thus, not necessarily reduce the variability, but it

would represent an even more realistic representation about the inherent uncertainty in the geologic system.

This can be illustrated by e.g. allowing the widths of the uniform PDFs for stresses to be increased to 8 and 12 MPa (i.e. between 37 and 45 MPa and 16–28 MPa), for the vertical and least horizontal direction, respectively comparing to the stresses shown in Table 2. This leads to a smoother curve from zero to 100% failure rate as displayed when comparing Fig. 11a and b. When using the 1% isocontour line – that can be used as a proxy for determining the safe injection envelope – the safe operation envelope would decrease.

5.5. Relevance of the approach application results to the injection site in focus and way forward

Very limited in-situ stress data were available for the region of the potential CO_2 injection site in focus (Nermoen et al., 2024). Actual data were only available for other geological formations and depths in the region. This made the evaluation of the in-situ stress-state conditions quite uncertain. Further evaluation is therefore required to determine the safe operating envelope and to determine the total amount of CO_2 to be injected for the site in focus. This knowledge gap may be filled in with additional field surveys including, but not limited to, well tests to estimate geomechanical properties and in-situ stresses such as LOT, XLOT tests during drilling new wells or mini-frac and step-rate tests for already drilled wells (Bohloli et al., 2014). Thus, this paper describes an approach which can help to move forward in the planning of injection pilots despite limited and uncertain data, while the large uncertainty with the input data for the site in focus calls for further studies of the field.

When maturing such projects towards designing pilot and full-scale 4D injection in fractured rocks, the question of how the presence of natural fractures may impact safety and injection limitations is to be addressed. The approach developed in this study was applied based on the results of geomechanical experiments for intact rock samples (Nermoen et al., 2024). Impact of presence of fractures and addressing geomechanics of fractured rock masses was not covered in this study. A potential approach to address these questions was discussed, indicating that the presence of fractures may significantly reduce the safe operating envelope. A rigorous study would be required, which may include laboratory experiments, modelling and upscaling approach and field studies for verification.

6. Conclusions

The paper outlined a methodology that leverages the uncertainty in input parameters stemming from natural geologic variability, experimental inaccuracies, and in-field stress estimates to assess geomechanical stability with probability. Special emphasis were put on the impact of cooling and re-pressurization due to the injection of cold CO_2. An Excel-based Monte Carlo model that sampled from estimated and experimentally derived probability density functions was implemented to estimate probability of failure as pressure and temperature is systematically varied. This model was applied to the data from the fractured carbonate oil and gas field (Nermoen et al., 2024).

Assuming the input uncertainty is true, we developed a pathway to realistically transfer the uncertainty through the analysis till an operational decision. This procedure eases the communication on uncertainty and risk for decision makers. The approach enables informed reservoir management decisions on how much CO_2 can be injected, the rate, and if pre-conditioning of the injected CO_2 should be performed to increase the total injection capacity.

The impact of cooling reduces the least principal stress and re-pressurization changes effective stresses. Both increased pressure and reduced temperature shift the stresses towards the failure. The stresses are evaluated in context with the strengths obtained from geomechanical tests via *qp*-plots.

The state of the reservoir operation is geomechanically stable if the stresses are within the failure envelope. As cooling and re-pressurization occur the number of unstable instances were counted enabling us to determine the probability of failure as function of pore pressure and temperature. If the risk appetite of the storage operator is given, the safe operating envelope can be determined. These factors have implications to further scenario developments related to pre-conditioning of CO_2 and total storage volume estimates.

Natural variability, either stemming from geological variation, experimental error, geological survival bias and its relation to strengths of rock masses, or related to uncertainty in Earth stresses, will always exist. All factors may all be crucial when evaluating the consequences of the decisions that needs to be made during operation. The model enables the user to use the uncertainty to develop mitigation plans before operation starts, and to develop tailor-made studies to maximize the value of new information during operation. The approach developed enables decision makers to communicate uncertainty in a precise way to stake holders, either that being local authorities, owners, or local communities. There will always be the need for subjective expert evaluation when performing geomechanical stability analyses due to limited

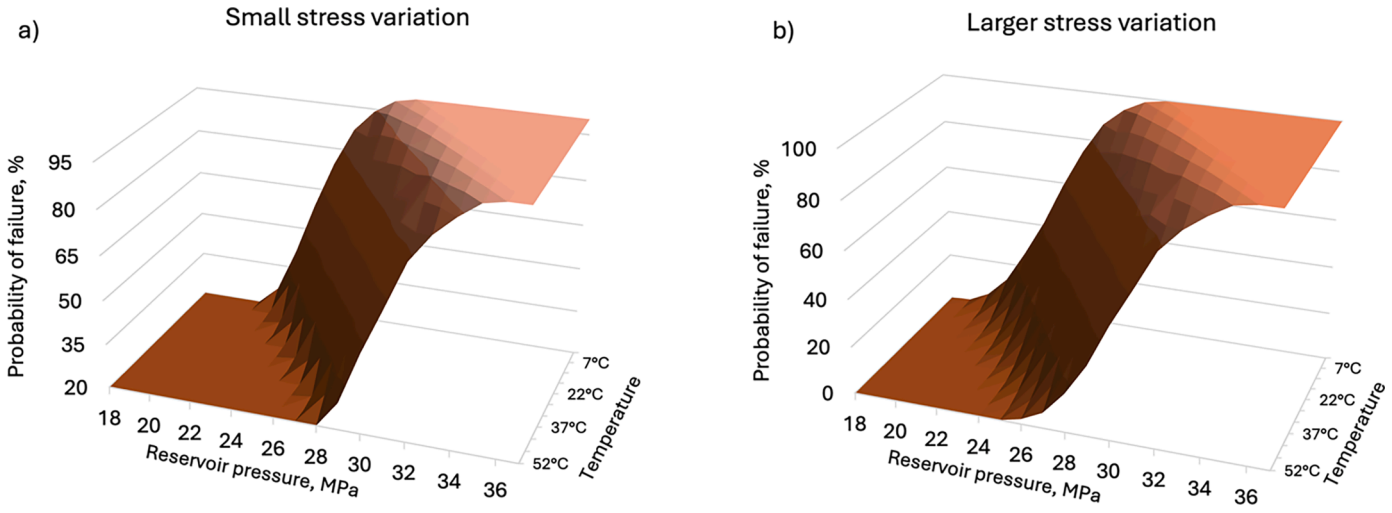

Fig. 11. a) Probability of re-opening tensile fractures as function of temperature and reservoir pressure for the same data shown in Fig. 8c using stress and rock parameters in Table 2. In b) the widths of the PDF for vertical and horizontal stresses were increased to 8 and 12 MPa, respectively.

number of data points required to calculate PDFs in a statistically stringent way. Moreover, often data sources overlap, thus calling for selections of what may be the most relevant data. The method developed here illustrate the practical consequences of these choices in a stringent way.

The approach developed in this study was used to evaluate the safe operating envelope using uncertain geomechanical parameters. The approach may be developed further to account for the effect of presence of natural fractures in rock masses, and to include this effect in assembling the failure envelopes. At the same time, a rigorous approach to evaluate the envelope for fractured rock masses rely on analysing of data on fractures, which is out of the scope of this paper. This may be the subject for the future studies.

CRediT authorship contribution statement

Anders Nermoen: Writing – original draft, Visualization, Validation, Supervision, Software, Project administration, Methodology, Investigation, Funding acquisition, Formal analysis, Data curation, Conceptualization. **Anton Shchipanov:** Writing – review & editing, Project administration, Methodology, Investigation. **Michal Matloch Porzer:** Writing – review & editing, Methodology, Investigation, Formal analysis, Data curation. **Jindřich Šancer:** Writing – review & editing, Investigation, Data curation. **Roman Berenblyum:** Writing – review & editing, Project administration, Funding acquisition.

Declaration of competing interest

The authors declare the following financial interests/personal relationships which may be considered as potential competing interests:

Anders Nermoen reports financial support was provided by The EEA and Norway Grants Fund for Regional Cooperation. If there are other authors, they declare that they have no known competing financial interests or personal relationships that could have appeared to influence the work reported in this paper.

Data availability

Data will be made available on request.

Acknowledgement

The results presented in this paper have been obtained within the CO2-SPICER project (CO_2 Storage Pilot In a CarbonatE Reservoir). The CO2-SPICER project benefits from a € 2.32 mil. grant from EEA - Norway Grants and Technology Agency of the Czech Republic TA ČR TO01000112. The project partners including Czech Geological Survey, MND, NORCE, VSB - Technical University of Ostrava and Institute of geophysics are thanked for providing input data for this study and fruitful discussions during preparation of the manuscript.

References

Alam, M., Fabricius, I., Christensen, H., 2012. Static and dynamic effective stress coefficient of chalk. Geophysics 77 (2). https://doi.org/10.1190/GEO2010-0414.1.

Archer, D., Brovkin, V., 2008. The millennial atmospheric lifetime of anthropogenic CO_2. Clim. Change 90, 283–297. https://doi.org/10.1007/s10584-008-9413-1.

Archer, D., Eby, M., Brovkin, V., Ridgwell, A., Cao, L., Mikolajewicz, U., Tokos, K., 2009. Atmospheric lifetime of fossil fuel carbon dioxide. Annu. Rev. Earth Planet. Sci. 37, 117–134. https://doi.org/10.1146/annurev.earth.031208.100206.

Barton, N.R., Lien, R., Lunde, J., 1974. Engineering classification of rock masses for the design of tunnel support. Rock Mech. Rock Eng. 6 (4), 189–236.

Berenblyum, R., Khrulenko, A., Kollbotn, L., Nermoen, A., Shchipanov, A., Skadsem, H., Hladik, V., 2017. Integrated approach to CO2 EOR and storage potential evaluation in an abandoned oil field in Czech Republic. In: 19th European Symposium on Improved Oil Recovery, 24-27 April. EAGE, Stavanger, Norway. https://doi.org/10.3997/2214-4609.201800046.

Bohloli, B., Skurtveit, E., Grande, L., Titlestad, G., Børresen, M., Johnsen, Ø., Braathen, A., 2014. Evaluation of reservoir and cap-rock integrity for the Longyearbyen CO2 storage pilot based on laboratory experiments and injection tests. Norweg. J. Geol. 94, 171–187.

Bourbiaux, B., Basquet, R., Cacas, M., Daniel, J., Sarda, S., 2002. An integrated workflow to account for multi-scale fractures in reservoir simulation models: implementation and benefits (SPE-78489). In: 10th Abu Dhabi international Petroleum Exhibition and Conference. SPE. https://doi.org/10.2118/78489-MS.

Dasgupta, P., 2021. The Economics of biodiversity: The Dasgupta Review. HM Treasury, London, UK. https://assets.publishing.service.gov.uk/media/602e92b2e90e07660f807b47/The_Economics_of_Biodiversity_The_Dasgupta_Review_Full_Report.pdf [Aquired: 1. November 2023].

Eberhardt, E., 2012. The Hoek-Brown Failure Criterion. Rock Mech. Rock Eng. 45, 981–988. https://doi.org/10.1007/s00603-012-0276-4.

Fjær, E., Holt, R., Horsrud, P., Raaen, A., Risnes, R., 2008. Petroleum related rock mechanics 2nd edition. In: Developments in Petroleum Science, 52. Elsevier Science Pub. Co., p. 491 m ISBN 978-0-44-50260-5.

Hladik, V., Procháč, R., Opletal, V., Pagác, M., Jirman, P., Berenblyum, R., Nermoen, A., 2021. CO2-SPICER - Czech-Norwegian project to prepare a CO2 storage pilot in a carbonate reservoir. In: Trondheim Conference on CO2 Capture, Transport and Storage. Trondheim, June 21-23: TCCS-11.

Hoek, E., Brown, E., 1997. Practical estimates of rock mass strength. Int. J. Rock Mech. Mining Sci. 38 (8), 1165–1186.

MND, 2023. Geometric geologic model of formations and faults. Personal Communication in the Project Team. CO2-SPICER project.

Nermoen, A., Berenblyum, R., Coussy, P., Guichet, X., Canteil, P., Orio, R., Roha, P., 2022. A techno-economic analysis tool for regional CO2 capture, transport, use and storage scenarios. In: Proceedings of the 16th International conference of greenhouse gas control technologies, 23-27 October. GHGT-16, Lyon, France.

Nermoen, A., Klempa, M., Porzer, M., Sancer, J., 2024. Geomechanical database of rock samples from the Zar-3 hydrocarbon and storage complex - petrophysics, stiffness, strength and effective stress estimate for stability evaluation during CO_2 storage. SSRN PREPRINT - Submitted. https://doi.org/10.2139/ssrn.4698108.

Nermoen, A., Korsnes, R., Christensen, H., Trads, N., Hiorth, A., Madland, M., 2013. In: Measuring the Biot stress coefficient and its implications on the effective stress estimate. *7th US Rock Mechanics /Geomechanics Symposium*. ARMA, San Francisco, CA, USA, pp. 1–9. *23-26 Juness*.

Newman, R., Noi, I., 2023. The global costs of extreme wather that are attributable to climate change. Nat. Commun. 14, 6103.

Olden, P., Jin, M., Pickup, G., Mackay, E., Hamilton, S., Somerville, J., Todd, A., 2014. Geomechanical Modeling of CO2 Geological Storage With the Use of Site Specific Rock Mechanics Laboratory data. *Petroleum Geoscience*. EAGE /The Geological Society of London. https://doi.org/10.1144/petgeo2012-048.

Park, J., Griffiths, L., Dautriat, J., Grande, L., Rodriguez, I., Iranpour, K., Best, A., 2022. Induced-seismicity geomechanics for controlled CO2 storage in the North Sea (IGCCS). Int. J. Greenhouse Gas Control 115, 103614. https://doi.org/10.1016/j.ijggc.2022.103614.

Parsonsova, A., Machar, I., 2021. National limits of sustainability: the Czech Republic's CO_2 emissions in the perspective of planetary boundaries. Sustainability 13 (4), 2164. https://doi.org/10.3390/su13042164.

Shchipanov, A., Kollbotn, L., Surguchev, L., Thomas, K., 2010. A new approach to deformable fractured reservoir: case Study of the Ekofisk Field (SPE 130425). In: SPE EUROPEC/EAGE Annual Conference and Exhibition. SPE, Barcelona, Spain. https://doi.org/10.2118/130425-MS. *14–17 June*.

Shchipanov, A., Nekrasov, A., Fonta, O., Potekhin, D., 2006. Modeling of fracturing of limestone petroleum reservoir using Fraca technology. In: 2nd EAGE St Petersburg International Conference and Exhibition on Geosciences. EAGE. https://doi.org/10.3997/2214-4609-pdb.20.P202.

Staš, L., Kolcun, A., Simkovicova, J., Soucek, K., 2003. Stress measurement in Carboniferous massif in eastern Czech part of Upper Silesian Basin and numerical model. In: Myrvoll, F. (Ed.), Field Measurements in Geomechanics Proceedings of the 6th International Symposium, 23-26 September. CRC Press, Oslo, Norway: London, pp. 361–368 ssISBN 978-9058096029.

Voake, T., 2020. Thermal Properties of reservoir rocks, role of pore fluids, minerals and diagenesis. A comparative study of two differently indurated chalks. PhD Dissertation Series At University of Stavanger (no. 494), pp. 1–120 ss.

Voake, T., Nermoen, A., Korsnes, R.I., Fabricius, I.L., 2024. Effect of Repeated Temperature Cycles On Thermal Expansion Coefficeint and Elastic Moduli of High Porosity Chalks. https://doi.org/10.2139/ssrn.4765327. *Preprint at SSRN*.

Voake, T., Nermoen, A., Korsnes, R., Fabricius, I., 2019. Temperature cycling and its effect on mechanical behaviours of high-porosity chalks. J. Rock Mech. Geotechn. Eng. (11), 749–759.

Zoback, M., Barton, C., Brudy, M., Castillo, D., Finkbeiner, T., Grollimund, B., Wiprut, D., 2003. Determination of stress orientation and magnitude in deep wells. Int. J. Rock Mech. Mining Sci. 40 (7–8), 1049–1076. https://doi.org/10.1016/j.ijrmms.2003.07.001. ISSN 1365-1609.

Zoback, M., Mastin, L., Barton, C., 1986. In-situ stress measurements. In: deep borehole using hydraulic fracturing, wellbore breakouts, and stonley wave plarization. *ISRM International Symposium*. OnePetro, Stockholm, Sweden. In: https://onepetro.org/ISRMIS/proceedings-abstract/IS86/All-IS86/ISRM-IS-1986-030/45467.